RSC Advances

ROYAL SOCIETY OF CHEMISTRY

www.rsc.org/advances

Journal Name

ARTICLE

An efficient Co-N-C oxygen reduction catalyst with highly dispersed Co sites derived from a ZnCo bimetallic zeolitic imidazolate framework

Received 00th January 20xx,
Accepted 00th January 20xx

DOI: 10.1039/x0xx00000x

www.rsc.org/

Xiaojuan Wang[a], Xinxin Fan[a], Honghong Lin[a], He Fu[a], Teng Wang[a], Jie Zheng[*a], Xingguo Li[*a]

In this work we report a highly efficient Co based catalyst for the oxygen reduction reaction (ORR) with highly dispersed Co sites on N-doped carbon. The catalyst is derived from a ZnCo bimetallic metal organic framework (MOF) by heat treatment in inert atmosphere at 1000 °C. Zn is simultaneously eliminated during the pyrolysis due to its high volatility at high temperature, yielding a highly porous structure with homogeneous Co loading. Another effect of Zn is to disperse Co in the MOF precursor, which effectively inhibits the aggregation of Co after pyrolysis. The best ORR performance is achieved when 5% Zn is substituted by Co in the MOF precursor. The resulted catalyst shows high half wave potential of 0.90 V *vs.* reversible hydrogen electrode in 0.1 M KOH solution, which is mainly attributed to the high dispersion of the ORR active Co sites.

Introduction

The oxygen reduction reaction (ORR) is the common cathode reaction in many important electric energy devices, such as fuel cells and metal air batteries.[1] The ORR is four electron process with sluggish kinetics and thus requires catalysts to enhance.[2] So far Pt-based catalysts are still the most efficient catalysts.[3] But the scarcity and high costs of platinum, together with instability and deactivation by CO poisoning and crossover effects, limit the application of fuel cells.[4] Currently there are tremendous efforts to develop efficient low cost ORR catalysts to replace Pt based noble metal catalysts to reduce the cost of these advanced electric energy devices.[5]

The M-N-C (M=Fe or Co) catalysts have been extensively studied as non-precious metal ORR catalysts.[6] According to previous studies, the ORR active sites are the N coordinated metal sites MN_x (M= Fe or Co, *x* is the average coordination number).[7] This type of ORR catalysts were first noted for the Co phthalocyanine complex.[8] Later, it was shown that high temperature pyrolysis of the Fe or Co complexes with metal-nitrogen bonding loaded on porous carbon results in more efficient and more robust M-N-C ORR catalysts.[6, 9] So far, there has been great progress in developing non-precious metal (NPM) ORR catalysts in alkaline media.[10] The ORR performance of several NPM catalysts is already comparable to or even better than that of the commercial Pt/C catalysts.[5a, 11] Despite of these progress, further improvement of the ORR performance of NPM catalysts is needed to meet the application target in fuel cells or metal-air batteries.

Metal organic frameworks (MOFs) contain atomically dispersed metal sites, which is an inherent advantage for catalysis.[12] However, direct application of MOFs in electrocatalysis is limited, as MOFs with good electron conductivity are extremely rare.[13] It has been found that pyrolysis of MOFs in inert atmosphere may lead to a large variety of carbon containing functional materials with good electron conductivity and more robust structure, which exhibit promising application in electrocatalysis and electrochemical energy storage. This approach is gaining increasing attention in recent years.[14] One type of widely used MOFs as precursors for ORR catalysts are zeolitic imidazolate frameworks (ZIFs) containing Fe or Co, in which Fe or Co cations are linked by imidazole type ligands. Owing to their inherent well defined M-N bonding structure, Fe or Co based ZIFs are highly attractive precursors to derive the M-N-C type ORR catalysts by pyrolysis. [9a, 14a-c, 14e] However, direct pyrolysis usually results in severe aggregation of the metal species [14a-e], which causes loss of the active MN_x sites.

In this work, we report a new strategy to prepare Co-N-C ORR catalysts with highly dispersed Co sites from a ZnCo bimetallic ZIF. Somehow surprising, very few literatures have studied the bimetallic ZIF with Zn^{2+} as one of metal cations.[15] Zn has relatively high vapor pressure and will evaporate at elevated temperature, leaving a highly porous carbon structure. Zn-based MOF is a very good precursors to derive porous carbon. Previous studies have shown that pyrolysis of

[a] Beijing National Laboratory for Molecular Sciences (BNLMS), The State Key Laboratory of Rare Earth Materials Chemistry and Applications, College of Chemistry and Molecular Engineering, Peking University, Beijing 100871, China. E-mail: xgli@pku.edu.cn, zhengjie@pku.edu.cn. Tel: 86-10-62765930. Fax: 86-10-62765930.

Electronic Supplementary Information (ESI) available: [photos and electrochemical curves of samples and tables of a comparison with the state of the art noble metal free ORR catalysts based on Co and N-containing carbons]. See DOI: 10.1039/x0xx00000x

Zn based MOFs, such as ZIF-8 and MOF-5, can generate highly porous carbon materials with little residual.[14h, 16] Thus, when the same pyrolysis procedure is applied to a ZnCo bimetallic ZIF with homogeneous distribution of the two metals, the aggregation of Co can be effectively inhibited as the Co species in the ZIF precursor is well dispersed by Zn which is removable after pyrolysis. Our results show that when 5% Zn in a Zn based ZIF (ZIF-8) is substituted by Co, very uniform Co distribution is achieved in the derived catalyst. The catalyst exhibits more positive onset potential, higher durability and methanol tolerance in alkaline electrolyte compared to the commercial Pt/C, which is mainly benefited from the high dispersion of the catalytic active Co sites.

Experimental

Materials and chemicals

Cobalt nitrate ($Co(NO_3)_2 \bullet 6H_2O$, >99%) and zinc nitrate ($Zn(NO_3)_2 \bullet 6H_2O$, >99%) were purchased from XILONG Chemicals (China). 2-Methylimidazole (mIm, 99%) was purchased from J&K Chemicals. The carbon supported platinum catalyst (Pt/XC-72, nominally 20 % on carbon black) was purchased from E-TEK, Ltd. Nafion (5 wt% solution in ethanol and water) was purchased from Alfa Aesar. All the reagents were used without further purification.

Synthesis of the catalysts

For convenience, the bimetallic ZIFs and the derived catalysts are designated as ZIF-(100-*x*)Zn*x*Co and C-(100-*x*)Zn*x*Co, respectively, where *x* is defined as the molar percentage of Co/(Co + Zn) in the starting materials.

We prepare the ZIF-(100-*x*)Zn*x*Co nanocrystals by a surfactant mediated growth method recently developed in our group.[17] The preparation is carried out in an aqueous emulsion composed of the metal nitrates with different Co/Zn ratio, mIm and surfactants. Typically, 1.5 g of mixture of surfactants (Span 80 and Tween 80 in weight ratio of 9:11) and 0.1 mol of 2-methylimidazole are dissolved in 300 mL of deionized water under sonication to give a homogeneous emulsion. 100 mL of mixed metal nitrate solution (zinc and cobalt, total 10 mmol metal) is poured into the emulsion. The solution is stirred at 60 °C for 4 h to give a turbid suspension. The ZIF-(100-*x*) Zn*x*Co nanocrystals are separated by centrifugation, washed three times with deionized water and two times with ethanol and then dried at 80 °C in vacuum for about 12 h.

The ORR catalysts are prepared by temperature programmed pyrolysis of the ZIF- (100-*x*)Zn*x*Co nanocrystals in Ar atmosphere. Typically, 0.5 g of the ZIF-(100-*x*)Zn*x*Co nanocrystals is heated to 1000 °C at 5 °C min^{-1} under an Ar stream in a tube furnace, then kept at the peak temperature for 60 min and allowed to cool down to room temperature.

Materials Characterization

X-ray diffraction (XRD, Rigaku D/max 200 diffractometer, Cu Kα), and high-resolution transmission electron microscopy (HRTEM, JEM 2100, 200 kV) are used to characterize the structure and morphology of products. The pore structure is analyzed by an Autosorb IQ gas sorption analyzer (Quantachrome) at 77 K. Before collecting nitrogen adsorption-desorption isotherms, samples are needed to be degassed at 200 °C for 2 h. The pore size distribution and surface area is obtained by the Brunauer–Emmett–Teller (BET) and Quenched Solid Density Functional Theory (QSDFT) methods assuming a slit/cylinder pores model, respectively. The X-ray photoelectron spectroscopy (XPS) analysis is conducted on an AXIS-Ultra spectrometer (Kratos Analytical) using monochromatic Al Kα radiation (225 W, 15 mA, 15 kV). An elemental analyzer (Vario EL) and Inductively Coupled Plasma-Atomic Emission Spectrometer (ICP-AES) are used to determine the content of C, H, N and metal content. Before elemental analyzer testing, all the samples are totally dried at 120 °C in a vacuum oven. Before ICP-AES analysis, the samples are first calcinated in air at 900 °C for 12 h and then the obtained residue are dissolved in 2 mol L^{-1} HNO_3 to give the solution for ICP-AES test.

Electrochemical Preparation and Characterization

To prepare the working electrode, 2 mg of samples are ultrasonically dispersed in a mixed solution of isopropanol and Nafion (0.5 wt%) ($V_{isopropanol}$:V_{nafion}=1:1) for about 1 h to make the concentration of 10 g L^{-1}. Then 7 μL suspension is dropped onto a rotating ring-disk electrode (RRDE, 5.61 mm of disk outer diameter, Platinum ring, Pine Research Instrumentation) surface and dried for 12 h at room temperature. The synthesized catalysts loading on RRDE is 0.28 mg cm^{-2}, respectively.

Cyclic voltammograms (CVs) and linear scan polarization curves (LSVs) are performed at room temperature in 0.1 M KOH. Prior to each measurement, the electrolyte is purged with argon or oxygen for at least 30 min. The electrochemical data is collected by a CHI 760D bipotentiostat. The reference electrode is a saturated calomel electrode (SCE). The potential are converted to the value versus reversible hydrogen electrode (RHE) to facilitate the comparison with literature. The counter electrode is a platinum foil. The LSVs results are subtracted by background current recorded in Ar-saturated electrolyte.

The number of electron transferred (n_e) during the ORR is calculated based on RRDE results. During the RRDE tests, the ring potential is set at 1.20 V *vs.* RHE in 0.1 M KOH. The n_e and peroxide yield H_2O_2% is calculated using the following equations[14a].

$$n_e = \frac{4I_d}{I_d + \frac{I_r}{N}} \quad \text{Equation 1}$$

$$H_2O_2\% = \frac{200I_r}{NI_d + I_r} \quad \text{Equation 2}$$

Where N=0.37 is the collection efficiency, I_d and I_r is the disk current and the ring current, respectively. Collection efficiency

of the ring electrode was calibrated by the $K_3Fe(CN)_6$ redox reaction.

Results and discussion

Structural and morphology characterization of the precursors

The Co based ZIF used in this work is ZIF-67, which is composed of Co cations bridged by 2-methylimidazole, as illustrated in Figure 1a. ZIF-67 has a Zn based isomorph ZIF-8 (Figure 1c). Therefore, it allows a continuous transition from ZIF-8 to ZIF-67 by different level of Co substitution. This substitution effect can be illustrated by replacing some of the CoN_4 tetrahedrons by the ZnN_4 ones (Figure 1b). The molar ratio of Co/(Zn+Co) in the ZIF-(100-*x*)Zn*x*Co is also calculated by ICP results, which is in good agreement with the value calculated by starting materials (Table S1).

TEM images (Figure 1d-f) reveals that the size of the ZIF-(100-*x*)Zn*x*Co nanocrystals is around 30 nm, showing little variation with the Co percentage. The samples exhibit gradually fading color from purple to white with decreasing Co percentage (Figure S1). We choose ZIF-95Zn5Co as a representative sample to make elemental mapping test, as seen in Figure 2a-d. Co and Zn mapping matches very well with the TEM image, indicating that the two metals are homogeneous distributed in the ZIF-95Zn5Co nanocrystals. As the isomorphous ZIF-67 and ZIF-8 have very similar lattice parameters,[18] the bimetallic ZIFs with different Co percentage have almost identical X-ray diffraction (XRD) patterns (Figure 2e), which are in excellent agreement with that of both ZIF-8 and ZIF-67.

We further study the chemical environment of the doped Co by XPS. As shown in Figure2f, the Co 2p spectra are almost identical for the Co-doped ZIF-8 and ZIF-67. The Co $2p_{3/2}$ peak is located at 780.8 eV, indicating that the incorporated Co is in the divalent state. By using the pure ZIF-67 sample as a reference, we can conclude that in the ZnCo bimetallic ZIF, the incorporated Co is also four fold coordinated by the N from the 2-methylimidazole ligand, almost identical to that in ZIF-67.

Structural and morphology characterization of the catalysts

The catalysts C-(100-*x*)Zn*x*Co are derived by pyrolysis of ZIF-(100-*x*)Zn*x*Co nanocrystals in Ar flow at 1000 °C for 1 h. After pyrolysis, most Zn will evaporate to yield a porous carbon structure and Co will remain in the structure. Elemental analysis suggests that the catalysts are composed of C, N and the corresponding metals (Table 1). Residual Zn can still be found, which is mainly due to the relatively short pyrolysis time compared to that in the literature.[14h, 16] The size and distribution of the Co species in the pyrolysis product can be tuned by the Co percentage *x*%.

C-100Zn is virtually nitrogen doped porous carbon (Figure 1i), with high specific surface area (SSA) more than 1000 m^2g^{-1} and rich microporosity (Figure 3, Table 1). Such structure is in good agreement with previous study on pyrolysis of ZIF-8.[14f-h] On the other hand, C-100Co contains many aggregated metal nanoparticles in addition to the N-doped carbon (Figure 1g), which is in agreement with the high Co content of 46 wt%. The SSA is only 231 m^2g^{-1}, as the residual Co particles block some of the pores. This is also in good agreement with previous studies on pyrolysis of ZIF-67 and other Co based MOFs.[14a-c]

The catalysts C-(100-*x*)Zn*x*Co with low *x* value exhibit very interesting structure features, as illustrated by C-95Zn5Co Similar to C-100Zn, it also shows a highly porous carbon structure without visible metal nanoparticles (Figure 1h). The absence of visible metal particles is carefully confirmed by high magnification TEM in more than 20 different locations of the sample. Under high magnification, only porous carbon structure can be observed (Figure 4a). C-(100-*x*)Zn*x*Co with low *x* value retain the merit of high SSA (>1000 m^2g^{-1}) and rich porosity (Figure 3, Table 1).

On the other hand, Co can be readily detected both macroscopically and microscopically. ICP result shows C-95Zn5Co contains 2.8 wt% Co (Table 1). Elemental mapping in TEM indicates that the distribution of Co is very homogeneous in this sample (Figure 4b-d). The above results suggest that Co does exist in this sample and must exist in a highly dispersed state.

A more detail structural characterization on the C-(100-*x*)Zn*x*Co catalysts with different *x* value is carried out. C-100Co exhibits well defined diffraction peaks corresponding to metallic Co (JCPDS No. 15-0806) in XRD (Figure 4e). The Co related peaks gradually vanish with decreasing *x*. For $x \leq 5$, only two broad peaks corresponding to graphite carbon centered at 25^o and 43^o are observed, indicating absence of crystalline Co in these samples. TEM study also suggests gradual diminishing of the metal particles with lower *x* (Figure 5). Compared to C-100Co, the Co nanoparticles become much sparser in C-90Zn10Co. When $x \leq 5$, no visible Co particles can be found. It is worth noting that visible Co particles in TEM disappear concomitantly with the Co related diffraction peaks in XRD.

XPS (Figure 4f) reveals different chemical environment of Co in C-(100-*x*)Zn*x*Co depending on *x*. The sharp peak at 778.3 eV and the broad peak at 780.6 eV are attributed to metallic and divalent Co, respectively. The metallic Co related peak only appears in C-100Co. XPS fails to detect metallic Co in C-90Zn10Co, though XRD and TEM suggest that there remain low density metallic Co particles (Figure 4f, Figure 5). This can be explained by the fact that XPS is only surface sensitive and tends to underestimate the metallic component embedded in the carbon matrix. Samples with even lower Co concentration only contain divalent Co, which is in agreement with the highly dispersed state suggested by XRD and TEM. The divalent nature of the highly dispersed Co species is attributed to the strong interaction between Co and the N doped carbon, preferably with the electron rich N sites.

The C-(100-*x*)Zn*x*Co samples also contain notable amount of nitrogen. The N 1s XPS spectra (Figure 6) of C-(100-*x*)Zn*x*Co exhibit three major components corresponding to pyridinic (397-399.5 eV), pyrrolic (400.2-400.9 eV) and graphitic (401-403 eV) nitrogen, which suggests that most N is incorporated into the carbon skeleton (Figure 6). In addition, including an additional component at 399-400.5 eV results in better fit. According to Jaouen *et. al.*, this component is attributed to the

nitrogen bonded to the metal,[19] which is in agreement with the considerable amount of divalent Co in C-(100-*x*)Zn*x*Co. Interestingly, this component becomes most prominent for *x*=1 and 5, in which Co is in the highly dispersed state according to the XRD and TEM results. This may further evidence that the highly dispersed Co should mainly exist in the form of CoN_x structure. In the ZIF precursor, the Co atoms are four fold coordinated by the N atoms. It is highly probable that the primary coordination environment of the Co atoms is largely preserved after pyrolysis. Previous X-ray absorption study on the pyrolysis product of a Co based ZIF suggested the existence of the CoN_x structure, though most Co is in the form of metallic particles.[14a]

The electrocatalytic performance of the catalysts

Figure 7 compares the ORR performance of the C-(100-*x*)Zn*x*Co catalysts with different *x* value. The cathodic current in the linear scanning voltammetry (LSV, Figure 7a) is resulted from the ORR on the catalysts. The catalytic activity is characterized by the onset potential (E_{onset}) and half-wave potential ($E_{1/2}$). Higher E_{onset} *and* $E_{1/2}$ value means lower overpotential for ORR or higher ORR activity. The $E_{1/2}$ value is 0.83 V *vs.* RHE for C-100Co. C-90Zn10Co shows little improvement in terms of $E_{1/2}$, while C-99Zn1Co and C-95Zn5Co exhibit a drastic positive shift in $E_{1/2}$ to 0.89-0.90 V *vs.* RHE, which is more positive compared to that of the commercial Pt/XC72 catalyst with 20 wt% Pt loading. Interestingly, further decreasing the Co percentage from 1 to 0 leads to poorer ORR performance. The $E_{1/2}$ value of C-100Zn is shifted to 0.79 V *vs.* RHE, even more negative than that of C-100Co. As summarized in Figure 7c, the $E_{1/2}$ value shows a non-monotonic dependence on the Co percentage *x*. Highest $E_{1/2}$ value is obtained when *x* = 1 and 5. The E_{onset} (Figure 7b) exhibits roughly the same trend, though the difference is much smaller.

Another criterion for ORR catalysts is the selectivity, which is given by the electron transfer number n_e and H_2O_2 yield. The ORR catalysts are preferably to have a four electron reduction process, *i.e.* directly reducing oxygen to water with minimum peroxide intermediate. The n_e value and H_2O_2 yield at a given potential can be obtained from a rotating ring disk electrode measurement (Figure 7a), [20] which is summarized in Figure 7a-b for different C-(100-*x*)Zn*x*Co samples. C-100Zn is superior to C-100Co in terms of n_e and H_2O_2 yield, though the latter shows more positive $E_{1/2}$ value. The n_e value and H_2O_2 yield at 0.4 V *vs.* RHE is 3.5 and 28% for C-100Co while is 3.7 and 15% for C-100Zn, respectively. Interestingly, the merit of high n_e and low H_2O_2 yield is maintained for the low Co percentage catalysts. The C-(100-*x*)Zn*x*Co samples ($0 \le x \le 5$) exhibit n_e value ~3.7 and H_2O_2 yield ~15%, similar to that of C-100Zn.

The dispersion of the ORR active metal sites is very important to further enhance the ORR performance. As demonstrated in this work, the enhanced Co dispersion drastically improves the ORR performance. With only 2.8 wt% Co, C-95Zn5Co apparently outperforms C-100Co with 46 wt% Co. On the other hand, lower Co percentage, though favours high Co dispersion, will lower the absolute density of the CoN_x active sites. The best catalytic performance is achieved for C-95Zn5Co, which contains the highest Co concentration while all the Co remains in the highly dispersed state. This catalyst is similar to C-99Zn1Co in terms of $E_{1/2}$ but shows much higher saturate current density due to higher density of the catalytically active Co sites (Figure 7a). The dependence of the ORR performance on *x* shown in Figure 7c is an excellent example showing the strong correlation between the ORR performance and the dispersion of the Co sites.

The residual Zn in the sample is inactive for ORR. In fact, Zn based catalysts have been rarely reported in ORR or similar redox processes. The ORR activity of C-100Zn is resulted from the N-doped carbon. [14f, 21] Recent studies suggest that N-doped carbon also exhibits certain ORR activity in alkaline electrolyte.[22] The enhancement of ORR activity are thought to a dipole effect, *i.e*. the doping of the nitrogen atom in the carbon materials lowers the electron density of the adjacent carbon atoms which is favourable to dissociative chemisorption of oxygen.[23] However, the N-doped carbon catalysts shows less active than the M-N-C catalysts (M= Fe or Co) with MN_x sites[24]. This is also clearly suggested by the significant improvement in $E_{1/2}$ when 0.1% Co is introduced into ZIF-8 (Figure 7). Therefore, the ORR activity of the C-(100-*x*)Zn*x*Co catalysts is mainly determined by the Co sites, despite of the residue Zn and N doping in the samples.

The C-95Zn5Co catalyst outperforms the commercial Pt/C catalyst with 20 wt% Pt loading in terms of the $E_{1/2}$ value. Although some noble metal free catalysts were reported to show lower overpotential than that of commercial Pt/C catalysts in alkaline electrolyte, our catalysts remain very impressive for its high ORR activity compared to these state of the art ORR catalysts.[25] As summarized in Table S2, compared to the state of the art Co based ORR catalysts, C-95Zn5Co is more than 50 mV lower in half-wave potential, which is benefited from the high dispersion of the Co sites. Furthermore, C-95Zn5Co also exhibits excellent stability after 5000 cycles and very strong tolerance to methanol (Figure S2). This catalyst, therefore, can be potentially used as a low cost alternative for Pt based ORR catalysts in alkaline electrolyte.

The strategy to obtain high Co dispersion here is particularly illuminating. Incorporation of Zn reduces the Co density in the ZIF structure and thus reduces the probability of aggregation during the pyrolysis. On the other hand, most Zn will evaporate after the high temperature treatment due to its high volatility. Therefore, in a high temperature pyrolysis process in inert atmosphere, Zn reduces the metal density by occupying the metal sites but without introducing a new metal component. It should also be noted that homogeneous distribution of Zn and Co in the bimetallic ZIF is critical to obtain the high dispersion of Co in the derived catalyst, which is facilitated by both the isomorphous nature of ZIF-67 and ZIF-8 and the surfactant mediated growth method. For comparison, a physical mixture of ZIF-8 and ZIF-67 prepared by ball milling results in inhomogeneous domains containing metallic Co nanoparticles in the pyrolysis products (Figure 8a). The ORR performance also shows no improvement compared to that of C-100Co (Figure 8b).

Conclusion

In conclusion, a ZnCo bimetallic ZIF with low Co percentage can be converted into a porous N-doped carbon supported catalyst with highly dispersed Co sites after pyrolysis. The catalyst contains homogeneously distributed Co species but without observable metallic Co particles, which is highly efficient in catalyzing the oxygen reduction reaction due to the high Co dispersion. The high dispersion is attributed to the volatility of Zn at high temperature, which reduces the Co density in the precursor but without introducing another metal phase after pyrolysis. The best ORR performance is achieved when 5% Zn is substituted by Co in the MOF precursor. The resulted catalyst shows high half-wave potential of 0.90 V *vs.* RHE in 0.1 M KOH solution. Many MOFs also have Zn based isomorphs. Using Zn based bimetallic MOFs for pyrolysis, therefore, can be employed as a general strategy to prepare carbon supported metal catalysts with high metal dispersion.

Acknowledgements

This study is supported by National Natural Science Foundation of China (No. U1201241, 11375020, 51431001 and 21321001).

Notes and references

1 (a) Y. Cao, Z. Wei, J. He, J. Zang, Q. Zhang, M. Zheng and Q. Dong, *Energy Environ. Sci.*, 2012, **5**, 9765-9768; (b) A. Rabis, P. Rodriguez and T. J. Schmidt, *ACS Catal.*, 2012, **2**, 864-890.

2 M. K. Debe, *Nature*, 2012, **486**, 43-51.

3 Y.-J. Wang, N. Zhao, B. Fang, H. Li, X. T. Bi and H. Wang, *Chem. Rev.*, 2015, **115**, 3433-3467.

4 Z. W. Chen, D. Higgins, A. P. Yu, L. Zhang and J. J. Zhang, *Energy Environ. Sci.*, 2011, **4**, 3167-3192.

5 (a) W. X. Yang, X. J. Liu, X. Y. Yue, J. B. Jia and S. J. Guo, *J. Am. Chem. Soc.*, 2015, **137**, 1436-1439; (b) W. Zhang, Z. Y. Wu, H. L. Jiang and S. H. Yu, *J. Am. Chem. Soc.*, 2014, **136**, 14385-14388; (c) Z.-S. Wu, S. Yang, Y. Sun, K. Parvez, X. Feng and K. Muellen, *J. Am. Chem. Soc.*, 2012, **134**, 9082-9085; (d) Y. Hou, Z. H. Wen, S. M. Cui, S. Q. Ci, S. Mao and J. H. Chen, *Adv. Funct. Mater.*, 2015, **25**, 872-882.

6 F. Jaouen, E. Proietti, M. Lefevre, R. Chenitz, J. P. Dodelet, G. Wu, H. T. Chung, C. M. Johnston and P. Zelenay, *Energy Environ. Sci.*, 2011, **4**, 114-130.

7 U. I. Kramm, J. Herranz, N. Larouche, T. M. Arruda, M. Lefevre, F. Jaouen, P. Bogdanoff, S. Fiechter, I. Abs-Wurmbach, S. Mukerjee and J.-P. Dodelet, *Phys. Chem. Chem. Phys.*, 2012, **14**, 11673-11688.

8 R. Jasinski, *Nature*, 1964, **201**, 1212-1213.

9 (a) A. Morozan and F. Jaouen, *Energy Environ. Sci.*, 2012, **5**, 9269-9290; (b) M. Bron, J. Radnik, M. Fieber-Erdmann, P. Bogdanoff and S. Fiechter, *J. Electroanal. Chem.*, 2002, **535**, 113-119.

10 (a) R. Jiang and D. Chu, *J. Power Sources*, 2014, **245**, 352-361; (b) Y. Jiao, Y. Zheng, M. Jaroniec and S. Z. Qiao, *Chem. Soc. Rev.*, 2015, **44**, 2060-2086.

11 (a) G. Zhang, W. Lu, F. Cao, Z. Xiao and X. Zheng, *J. Power Sources*, 2016, **302**, 114-125; (b) Y. Liu, J. Li, W. Li, Y. Li, Q. Chen and F. Zhan, *J. Power Sources*, 2015, **299**, 492-500.

12 (a) A. Corma, H. Garcia and F. X. L. I. Llabres i Xamena, *Chem. Rev.*, 2010, **110**, 4606-4655; (b) J. Lee, O. K. Farha, J. Roberts, K. A. Scheidt, S. T. Nguyen and J. T. Hupp, *Chem. Soc. Rev.*, 2009, **38**, 1450-1459.

13 D. M. D'Alessandro, J. R. R. Kanga and J. S. Caddy, *Aust. J. Chem.*, 2011, **64**, 718-722.

14 (a) S. Q. Ma, G. A. Goenaga, A. V. Call and D. J. Liu, *Chem.-Eur. J.*, 2011, **17**, 2063-2067; (b) X. Wang, J. Zhou, H. Fu, W. Li, X. Fan, G. Xin, J. Zheng and X. Li, *J. Mater. Chem. A*, 2014, **2**, 14064-14070; (c) W. Xia, J. Zhu, W. Guo, L. An, D. Xia and R. Zou, *J. Mater. Chem. A*, 2014, **2**, 11606-11613; (d) V. P. Santos, T. A. Wezendonk, J. J. D. Jaén, A. I. Dugulan, M. A. Nasalevich, H.-U. Islam, A. Chojecki, S. Sartipi, X. Sun, A. A. Hakeem, A. C. J. Koeken, M. Ruitenbeek, T. Davidian, G. R. Meima, G. Sankar, F. Kapteijn, M. Makkee and J. Gascon, *Nat Commun*, 2015, **6**, 6451; (e) D. Zhao, J.-L. Shui, C. Chen, X. Chen, B. M. Reprogle, D. Wang and D.-J. Liu, *Chem. Sci.*, 2012, **3**, 3200-3205; (f) A. Aijaz, N. Fujiwara and Q. Xu, *J. Am. Chem. Soc.*, 2014, **136**, 6790-6793; (g) W. Chaikittisilp, M. Hu, H. Wang, H. S. Huang, T. Fujita, K. C. Wu, L. C. Chen, Y. Yamauchi and K. Ariga, *Chem. Commun.*, 2012, **48**, 7259-7261; (h) B. Liu, H. Shioyama, H. L. Jiang, X. B. Zhang and Q. Xu, *Carbon*, 2010, **48**, 456-463.

15 A. Schejn, A. Aboulaich, L. Balan, V. Falk, J. Lalevee, G. Medjahdi, L. Aranda, K. Mozet and R. Schneider, *Catalysis Science & Technology*, 2015, **5**, 1829-1839.

16 (a) H.-L. Jiang, B. Liu, Y.-Q. Lan, K. Kuratani, T. Akita, H. Shioyama, F. Zong and Q. Xu, *J. Am. Chem. Soc.*, 2011, **133**, 11854-11857; (b) G. Srinivas, V. Krungleviciute, Z.-X. Guo and T. Yildirim, *Energy Environ. Sci.*, 2014, **7**, 335-342.

17 X. Fan, W. Wang, W. Li, J. Zhou, B. Wang, J. Zheng and X. Li, *Acs Appl. Mater. Interfaces*, 2014, **6**, 14994-14999.

18 R. Banerjee, A. Phan, B. Wang, C. Knobler, H. Furukawa, M. O'Keeffe and O. M. Yaghi, *Science*, 2008, **319**, 939-943.

19 F. Jaouen, J. Herranz, M. Lefevre, J.-P. Dodelet, U. I. Kramm, I. Herrmann, P. Bogdanoff, J. Maruyama, T. Nagaoka, A. Garsuch, J. R. Dahn, T. Olson, S. Pylypenko, P. Atanassov and E. A. Ustinov, *Acs Appl. Mater. Interfaces*, 2009, **1**, 1623-1639.

20 M. Lefèvre and J.-P. Dodelet, *Electrochim. Acta*, 2003, **48**, 2749-2760.

21 P. Zhang, F. Sun, Z. Xiang, Z. Shen, J. Yun and D. Cao, *Energy Environ. Sci.*, 2013, **7**, 442-450.

22 K. Gong, F. Du, Z. Xia, M. Durstock and L. Dai, *Science*, 2009, **323**, 760-764.

23 J. Masa, W. Xia, M. Muhler and W. Schuhmann, *Angew. Chem. Int. Ed.*, 2015, **54**, 10102-10120.

24 (a) X. Wang, H. Fu, W. Li, J. Zheng and X. Li, *RSC Adv.*, 2014, **4**, 37779-37785; (b)J. Masa, A. Zhao, W. Xia, Z. Sun, B. Mei, M. Muhler and W. Schuhmann, *Electrochem. Commun.*, 2013, **34**, 113-116; (c) L. Wang, A. Ambrosi and M. Pumera, *Angew. Chem. Int. Ed.*, 2013, **52**, 13818-13821.

25 (a) Y. Wu, Q. Shi, Y. Li, Z. Lai, H. Yu, H. Wang and F. Peng, *J. Mater. Chem. A*, 2015, **3**, 1142-1151; (b) M. Li, X. Bo, Y. Zhang, C. Han, A. Nsabimana and L. Guo, *J. Mater. Chem. A*, 2014, **2**, 11672-11682; (c) Z.-Y. Wu, P. Chen, Q.-S. Wu,

L.-F. Yang, Z. Pan and Q. Wang, *Nano Energy*, 2014, **8**, 118-125.

Journal Name

ARTICLE

Table 1 The elemental content and BET surface area (S_{BET}) of the C-(100-*x*)Zn*x*Co ORR catalysts.

Sample	C (wt%)	N (wt%)	H (wt%)	Zn (wt%)	Co (wt%)	S_{BET} ($m^2 g^{-1}$)
C-100Co	40.58	3.21	0.95	0	46.2	231
C-90Zn10Co	78.81	3.31	1.68	0.164	7.13	674
C-95Zn5Co	79.57	3.32	2.90	0.004	2.80	1132
C-99Zn1Co	81.96	4.53	2.02	0.464	2.60	1288
C-99.9Zn0.1Co	74.59	7.90	2.20	4.150	0.05	1112
C-100Zn	73.89	7.76	2.12	5.011	0	1049

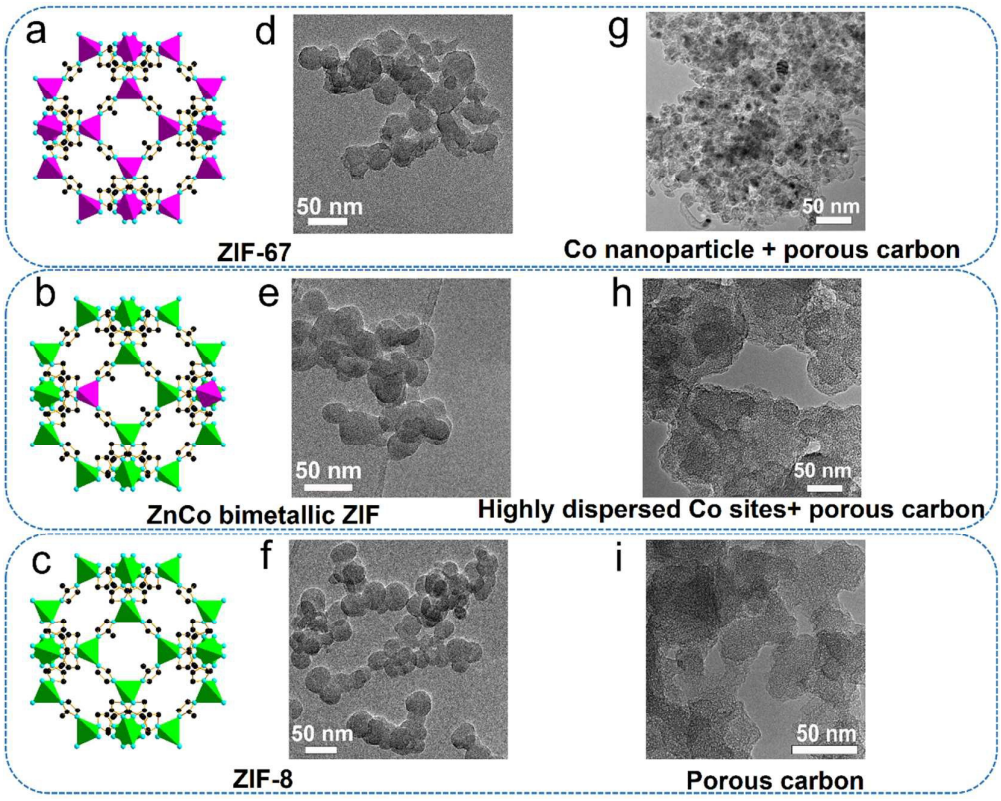

Figure 1 Crystal structures (a-c) and TEM images (d-f) of ZIF-67, ZnCo bimetallic ZIF (ZIF-95Zn5Co) and ZIF-8 and TEM images (h-g) of the corresponding catalysts derived by pyrolysis. The green and purple tetrahedrons represent the ZnN_4 and CoN_4 structures, respectively.

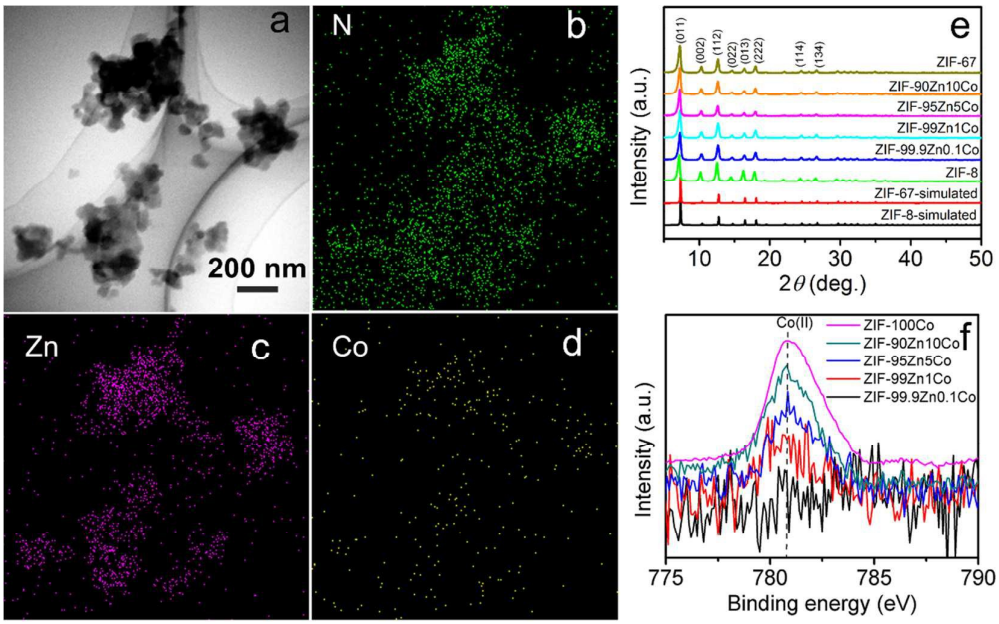

Figure 2 Analysis of 95Zn5Co. (a) A bright field TEM image; (b-d) Nitrogen, zinc and cobalt mapping of the corresponding region in (a); (e) XRD patterns of ZIF-(100-*x*)Zn*x*Co; (f) High resolution Co $2p_{3/2}$ XPS spectra of ZIF-(100-*x*)Zn*x*Co.

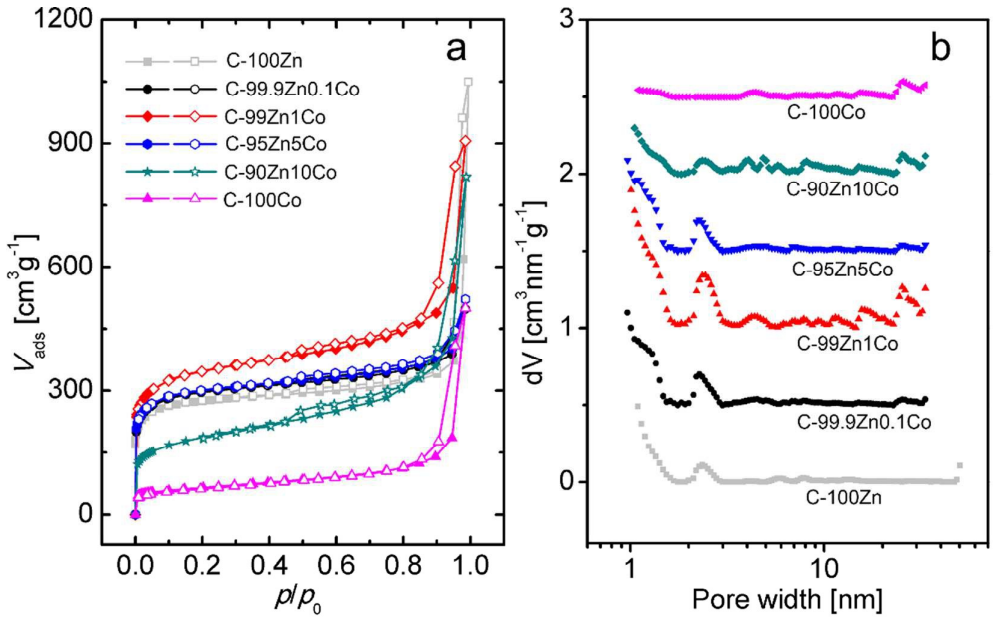

Figure 3 Nitrogen adsorption-desorption isotherms (a) and pore size distributions (b) of the C-(100-*x*) Zn*x*Co samples.

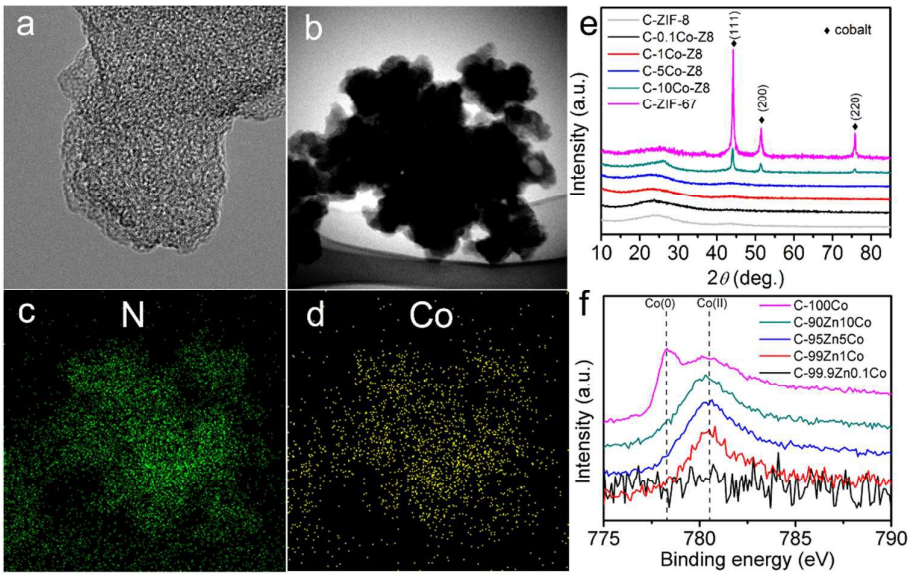

Figure 4 Analysis of C-95Zn5Co. (a) A high magnification TEM image, showing absence of metal particles; (b) A bright field TEM image in the scanning TEM mode; (c-d) Nitrogen and cobalt mapping of the corresponding region in (b), showing homogeneously distributed N and Co. (e) XRD patterns of C-(100-*x*)Zn*x*Co; (f) High resolution Co $2p_{3/2}$ XPS spectra of C-(100-*x*)Zn*x*Co. In the Figure 4e, the intensity of the six patterns are normalized with respect to the graphitic peak at 25°.

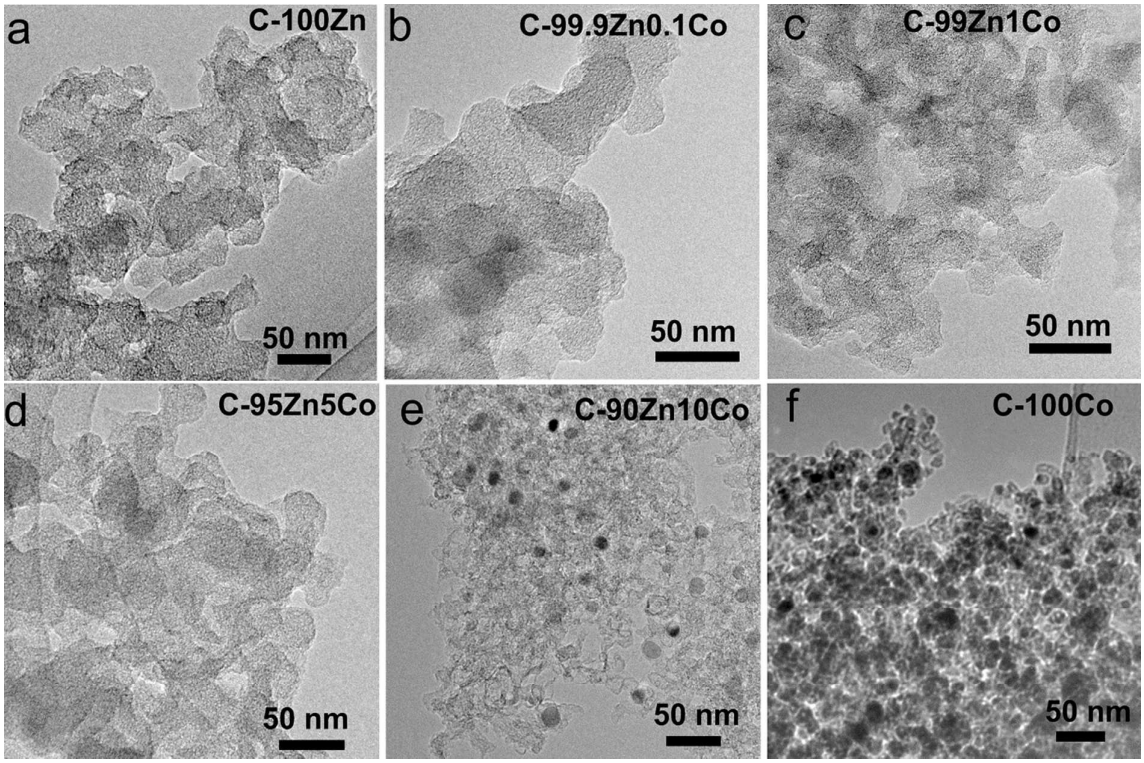

Figure 5 TEM images of C-(100-x) ZnxCo. When x≥10, the visible cobalt particles occur.

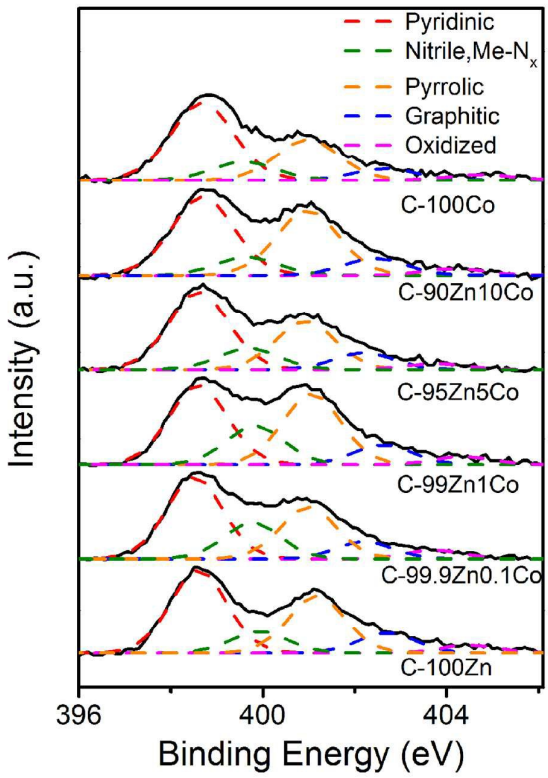

Figure 6 High resolution N 1s XPS spectra of C-(100-*x*)Zn*x*Co.

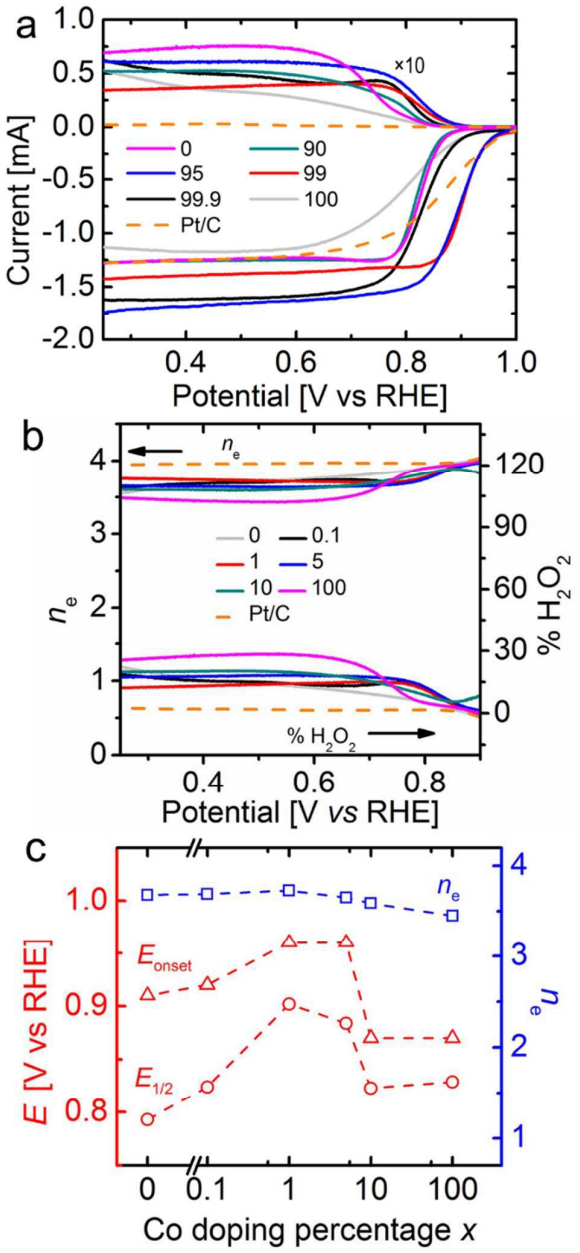

Figure 7 (a) The linear scan voltammetry of C-(100-*x*)Zn*x*Co in O_2-saturated 0.1 M KOH measured on a rotating ring disk electrode (RRDE) at the rotating rate of 1600 rpm with a scan rate of 10 mVs^{-1}, where *x* is the molar fraction of Co/(Co + Zn) in the starting materials. A commercial Pt/C catalyst with 20 wt% Pt loading is used as the reference material. (b) Summary of H_2O_2 yield and electron transfer number (n_e) in alkaline electrolytes. (c) The onset potential (E_{onset}), half-wave potential ($E_{1/2}$) and the electron transfer number (n_e) at 0.4 V *vs.* RHE for different Co percentage *x*.

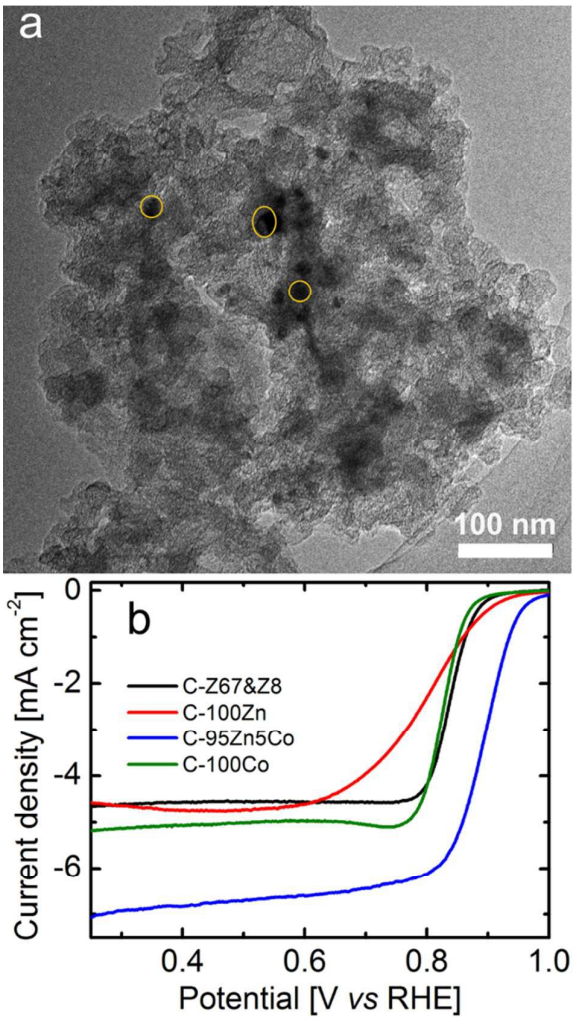

Figure 8 (a) TEM image of the catalyst C-Z67&Z8 derived from a physical mixture of ZIF-8 and ZIF-67 (molar ratio Co/(Zn+Co)=0.05. The domains in the orange cycles are aggregated cobalt. (b) Polarization curves of the catalyst C-Z67&Z8 derived from a physical mixture of ZIF-8 and ZIF-67 (molar ratio Co/(Zn+Co)=0.05), C-100Zn, C-95Zn5Co and C-100Co.

Highly dispersed Co sites loaded on the porous N-doped carbon is obtained by pyrolysis of ZnCo bimetallic ZIF with low Co percentage, which exhibits excellent catalytic performance for the electrocatalytic oxygen reduction reaction (ORR).